Characterization of Ultraflat Titanium Oxide Surfaces

Paola Cacciafesta,[†,‡] Keith R. Hallam,[§] Caroline A. Oyedepo,[§]
Andrew D. L. Humphris,[‡] Mervyn J. Miles,[‡] and Klaus D. Jandt*,[†,||]

Department of Oral and Dental Science, Biomedical Engineering and Biomaterials Science Section, University of Bristol, Lower Maudlin Street, Bristol BS1 2LY, U.K., H. H. Wills Physics Laboratory, University of Bristol, Tyndall Avenue, Bristol BS8 1TL, U.K., Interface Analysis Centre, Oldbury House, University of Bristol, 121 St. Michael's Hill, Bristol BS2 8BS, U.K., and Department of Materials Science and Engineering, Technisches Institut, Friedrich-Schiller-Universität Jena, Löbdergraben 32, D-07743 Jena, Germany

Received August 7, 2001. Revised Manuscript Received November 5, 2001

In this work we investigated the physical and chemical nature of ultraflat titanium dioxide (TiO_2) samples which we had previously used as substrates for the investigation of adsorbed protein molecules (Cacciafesta, P.; Humphris, A. D. L.; Jandt, K. D.; Miles, M. J. *Langmuir* **2000**, *16*, 8167). Titanium films were prepared by thermal evaporation on a heated mica surface and either separated from the mica to investigate the resulting surface or left in contact with the mica to analyze the titanium−mica interface. Atomic force microscopy (AFM) of the surfaces exposed after removal of the mica showed very flat surfaces [root-mean-square roughness of 0.29 nm ± 0.03 nm] and the presence of disordered as well as ordered structures. Different degrees of order were observed, such as a square lattice with spacing of $a_0 = 0.49$ nm, a regular pattern with spacings of $a_0 = 0.47$ nm and $b_0 = 0.35$ nm with an angle of ∼80° between a_0 and b_0, or the presence of surface defects. These ordered structures were not stable upon long-term AFM imaging and could be damaged by the scanning tip. To further investigate the nature of the ordered regions, X-ray diffraction (XRD) was performed for the titanium−mica samples. XRD showed the crystalline structures of both the mica and the titanium film but did not detect any order in the titanium−mica interface. Possible causes for the formation of the ordered regions are discussed, in the cases of formation both after removal of mica or during sample preparation. The chemical nature of the titanium−mica interface was investigated with secondary ion mass spectrometry and X-ray photoelectron spectroscopy (XPS) via depth profiling of the titanium−mica samples from the titanium side. The metal film was found to be mainly composed of titanium and to a lesser extent of oxygen and carbon. After the metal film was sputtered and the titanium−mica interface was reached, the titanium concentration decreased and the concentration of the typical mica elements, such as silicon, aluminum, and potassium, increased. XPS was also used to investigate the chemical composition of the surfaces obtained after mica removal, which were found to be mainly composed of TiO_2 with a small percentage of Ti_2O_3. The possible applications of this simple method for preparing ultraflat TiO_2 surfaces are discussed.

Introduction

Titanium is highly reactive with oxygen and readily forms a surface oxide layer when exposed to oxygen.[1] This oxide layer primarily consists of titanium dioxide TiO_2, though Ti_2O_3 and other forms may also be present.[1,2] TiO_2 can exist in three crystalline phases, rutile, anatase, and brookite, or can be amorphous.[3,4] The spontaneously forming native oxide is amorphous at room temperature and has a thickness of 2−6 nm.[1] The crystalline phases form at higher temperatures, and the transition temperatures from one crystalline form to another vary with the preparation method. For example, on TiO_2 thin films prepared by atomic layer deposition, amorphous films grow below 440 K, whereas the anatase structure is predominant at 440−625 K and rutile above 625 K.[5] TiO_2 thin films prepared by metal−organic chemical vapor deposition (MOCVD) show the anatase−rutile transition at 670 K.[6] For sputter-deposited TiO_2 films, the amorphous structure is observed at temperatures below 570 K,[7,8] the anatase

* Corresponding author. Phone: +49 3641 947730. Fax: +49 3641 947732. E-mail: Klaus.jandt@uni-jena.de.
† Department of Oral and Dental Science, Biomedical Engineering and Biomaterials Science Section.
‡ H. H. Wills Physics Laboratory.
§ Interface Analysis Centre, Oldbury House.
|| Friedrich-Schiller-Universität Jena.

(1) Kasemo, B. *J. Prosthet. Dent.* **1983**, *49*, 832.
(2) Lausmaa, J. *J. Electron Spectrosc. Relat. Phenom.* **1996**, *81*, 343.
(3) Pearson, W. B. *A Handbook of Lattice Spacings and Structures of Metals and Alloys*; Pergamon Press: London, U.K., 1967; Vol. 2.
(4) Henrich, V. E.; Cox, P. A. *The Surface Science of Metal Oxides*; Cambridge University Press: Cambridge, U.K., 1994.
(5) Aarik, J.; Aidla, A.; Uustare, T.; Sammelselg, V. *J. Cryst. Growth* **1995**, *148*, 268.
(6) Byun, C.; Jang, J. W.; Kim, I. T.; Hong, K. S.; Lee, B. W. *Mater. Res. Bull.* **1997**, *32*, 431.
(7) Gasgnier, M.; Lagnel, F.; Poumellec, B.; Marucco, J. F. *Thin Solid Films* **1990**, *187*, 25.

10.1021/cm0112183 CCC: $22.00 © 2002 American Chemical Society
Published on Web 01/22/2002

Table 1. Crystal Structures of Titanium and the Most Common Forms of Titanium Oxides [from Ref 3]

	system	a_0 [nm]	b_0 [nm]	c_0 [nm]
titanium	hexagonal	0.295		0.4686
TiO_2 rutile	tetragonal	0.459373		0.295812
TiO_2 anatase	tetragonal	0.3785		0.9514
TiO_2 brookite	orthorhombic	0.9185	0.5447	0.5145
Ti_2O_3	hexagonal	0.5148		1.3642

structure is predominant at 570−770 K,[9] and the rutile structure appears above 870 K.[9] The transition temperatures and, hence, the transition from one crystalline form of TiO_2 to another can be decreased by chemical doping[10−12] or alcohol (butanol) washing.[13] A recent study reported the micropatterning of anatase TiO_2 films on a self-assembled monolayer surface by a sol−gel technique that does not require posttreatment heat curing.[14] The crystal structures of pure titanium and the several forms of titanium oxides have been investigated, and the space group and unit cell parameters of each form have been characterized.[3] Table 1 reports the crystal structure and parameters of pure titanium and its most common oxidized forms.

The surface properties of TiO_2 make it suitable for a number of applications. In medicine and dentistry, titanium is used for cardiovascular devices and dental and orthopedic implants.[15] The passivating properties of TiO_2 make the titanium implants resistant to corrosion from the environment and prevent ion release from the implant into the body.[16] Its high strength and low density make the implants light and fatigue-resistant.[16] Other properties, such as the high refractive index of TiO_2[16] and its low adsorption coefficient,[16] make it an ideal material for optical coatings.[17] Its photoactive potential and photocatalytic activity[18] are exploited for practical applications such as the photocleavage of water,[19] photocatalytic decomposition of organics,[20,21] and solar energy conversion.[22−24]

A study of the adsorption of chemical species on TiO_2 surfaces is clearly of critical importance in a number of fields and requires the application of high-sensitivity analytical techniques.

For the direct visualization of adsorbed molecules, some of the most sensitive surface techniques are to be found in the family of scanning probe microscopies (SPMs), of which two well-known examples are scanning tunneling microscopy[25] and atomic force microscopy (AFM).[26] SPMs can achieve atomic resolution of surfaces and molecules adsorbed on a surface.[27] However, to image atomic- or molecular-size features, an essential prerequisite is an extremely flat surface. If the substrate presents any topographic feature that is comparable or larger than the adsorbed molecule, the latter will be "hidden" by the topography because AFM images are height-sensitive. Because the average dimensions of the molecules under investigation, such as proteins or organic adsorbates, are in the order of nanometers in size, the root-mean-square (rms) roughness of the ideal substrate should equally be in the order of a few nanometers or less.

Flat TiO_2 surfaces are commercially available in different crystalline structures but at relatively great expense. To avoid this, flat TiO_2 surfaces can be prepared in-house using one of the following techniques: sputtering;[28,29] chemical vapor deposition;[30] anodic growth;[31] modification of a single TiO_2 crystal by polishing, lapping, chemical etching, or doping;[32] deposition of TiO_2 thin layers from sol−gel precursors on self-assembled monolayers patterned by microcontact printing techniques;[33] or thermal evaporation onto a flat substrate, such as mica,[34] a single sodium chloride crystal,[35] or another smooth crystal or metal.[36]

In a previous paper,[37] we reported a simple and economic method for preparing ultraflat TiO_2 surfaces and used them as substrates for AFM investigation of adsorbed human plasma fibrinogen at molecular and submolecular resolution. Because these surfaces are intended to model the chemical properties of biomaterial surfaces, such as titanium implants, their surface chemical composition should be similar to clinically used titanium implant surfaces. It has been shown that surface properties, such as topography, crystallinity, microstructure, oxide thickness, and composition of the contamination layer, of titanium differ widely according to the preparation method and applied finishing treatments (e.g., exposure to air, electropolishing, cleaning procedure, and sterilization).[2] It is, therefore, pertinent to characterize any titanium surface prepared by new

(8) Meng, L. J.; Andritschky, M.; dos Santos, M. P. *Appl. Surf. Sci.* **1993**, *65/66*, 235.
(9) Williams L. M.; Hess, D. W. *J. Vac. Sci. Technol. A* **1983**, *1*, 1810.
(10) Kittaka, S.; Matsuno, K.; Takahara, S. *J. Solid State Chem.* **1997**, *132*, 447.
(11) Vargas, S.; Arroyo, R.; Haro, E.; Rodriguez, R. *J. Mater. Res.* **1999**, *14*, 3932.
(12) Gennari, F. C.; Pasquevich, D. M. *J. Am. Ceram. Soc.* **1999**, *82*, 1915.
(13) Ha, P. S.; Youn, H. J.; Jung, H. S.; Hong, K. S.; Park, Y. H.; Ko, K. H. *J. Colloid Interface Sci.* **2000**, *223*, 16.
(14) Koumoto, K.; Seo, S.; Sugiyama, T.; Seo, W. S.; Dressick, W. J. *Chem. Mater.* **1999**, *11*, 2305.
(15) Kasemo, B.; Lausmaa, J. *Crit. Rev. Biocompat.* **1986**, *4*, 335.
(16) Kasemo, B.; Lausmaa, J. In *Tissue Integrated Prostheses: Osseointegration in Clinical Practice*; Brånemark, P.-I., Zarb, G. A., Albrektsson, T., Eds.; Quintessence: Chicago, IL, 1985; p 99.
(17) Piccirillo, A.; Moro, L.; Natta, D.; Re, D.; Lazzeri, P. *Microelectron. J.* **1994**, *25*, 589.
(18) Wold, A. *Chem. Mater.* **1993**, *5*, 280.
(19) Fujishima, A.; Honda, K. *Nature* **1972**, *238*, 37.
(20) Pelizzetti, E.; Minero, C.; Carlin, V.; Borgarello, E. *Chemosphere* **1992**, *25*, 343.
(21) Kesselman, J. M.; Shreve, G. A.; Hoffmann, M. R.; Lewis, N. S. *J. Phys. Chem.* **1994**, *98*, 13385.
(22) Hagfeldt, A.; Gratzel, M. *Chem. Rev.* **1995**, *95*, 49.
(23) Gratzel, M. *P. Proc., Indian Acad. Sci., Chem. Sci.* **1995**, *107*, 607.
(24) Arango, A. C.; Johnson, L. R.; Bliznyuk, V. N.; Schlesinger, Z.; Carter, S. A.; Horhold, H. H. *Adv. Mater.* **2000**, *12*, 1689.
(25) Binnig, G.; Rohrer, H.; Gerber, C.; Weibel, E. *Appl. Phys. Lett.* **1982**, *40*, 178.
(26) Binnig, G.; Quate, C. F.; Gerber, C. *Phys. Rev. Lett.* **1986**, *56*, 930.
(27) Ohnesorge, F.; Binnig, G. *Science* **1993**, *260*, 1451.
(28) Porta, G. M.; Rancourt, J. D.; Taylor, L. T. *Chem. Mater.* **1991**, *3*, 423.
(29) Ting, C. C.; Chen, S. Y.; Liu, D. M. *J. Appl. Phys.* **2000**, *88*, 4628.
(30) Battiston, G. A.; Gerbasi, R.; Gregori, A.; Porchia, M.; Cattarin, S.; Rizzi, G. A. *Thin Solid Films* **2000**, *371*, 126.
(31) Vasilescu, E.; Drob, P.; Popa, M. V.; Anghel, M.; Lopez, A. S.; Mirza-Rosca, I. *Mater. Corros.* **2000**, *51*, 413.
(32) Miki, T.; Yanagi, H. *Langmuir* **1998**, *14*, 3405.
(33) Jeon, N. L.; Clem, P. G.; Nuzzo, R. G.; Payne, D. A. *J. Mater. Res.* **1995**, *10*, 2996.
(34) Jobin, M.; Taborelli, M.; Descouts, P. *J. Appl. Phys.* **1995**, *77*, 5149.
(35) Zenhausern, F.; Adrian, M.; Descouts, P. *Colloids Surf. B* **1993**, *1*, 133.
(36) Grunwaldt, J. D.; Gobel, U.; Baiker, A. *Fresenius' J. Anal. Chem.* **1997**, *358*, 96.
(37) Cacciafesta, P.; Humphris, A. D. L.; Jandt, K. D.; Miles, M. J. *Langmuir* **2000**, *16*, 8167.

methods. The aim of the present work was to carry out an investigation of the surface and bulk properties of our specially prepared ultraflat samples, including the chemical composition, the distribution, and occurrence of different oxide forms and their crystalline or amorphous structure. AFM, X-ray diffraction (XRD), dynamic secondary ion mass spectrometry (SIMS), and X-ray photoelectron spectroscopy (XPS) were used for the physicochemical characterization of the samples.

Materials and Methods

Sample Preparation. The "template stripping" method developed by Hegner et al.[38] was modified to obtain atomically flat surfaces of titanium and its oxides. Muscovite mica was purchased from Agar Scientific Ltd. (Stansted, U.K.) and titanium from Goodfellow Cambridge Ltd. (Huntingdon, U.K.) in the form of a wire of >99.6% purity, as stated by the manufacturer.

A freshly cleaved mica surface was placed in a vacuum chamber (Edwards vacuum system E306A, Crawley, U.K.) and heated to a temperature of 573 K for 5 h at a pressure below 10^{-4} Pa. The in-house heating stage was based on a high-purity oxygen-free copper block with halogen bulbs in thermal contact. A 200 nm layer of titanium was thermally evaporated onto the mica surface at a rate of ~0.1 nm/s from a tungsten filament. The deposition rate was derived from a previous calibration of the system preparing metal films at different filament currents and measuring the total evaporation time and the film thickness. The film was then allowed to anneal on the heating stage at 573 K for 12 h. Once cooled and removed from the vacuum chamber, the mica−titanium substrate was glued on the titanium face onto a glass support using epoxy resin (Epoxy Technology, Chelmsford, MA) and cured at a temperature of 423 K for 1 h. The titanium surfaces were then stored in a plastic Petri dish and only exposed when required. The mica layers were mechanically removed to allow investigation of the exposed titanium surfaces with AFM and XPS, whereas the mica layers were left on the titanium film when analyzing the mica−titanium interface using XRD, SIMS, and XPS depth profiling. XRD analysis was performed from the mica side of the samples. SIMS and XPS depth profiling were performed from the titanium side of samples not glued to a glass support.

AFM. A Nanoscope IIIa AFM (Digital Instruments, Santa Barbara, CA) equipped with a 12 μm piezoscanner (E scanner) was used for imaging the samples at room temperature. The maximum image size used was 1 μm × 1 μm, and imaging was carried out at different sample locations to ensure reproducibility. After mechanical removal of mica, the titanium surfaces were immediately loaded into the AFM and imaged in air using a contact mode with Si_3N_4 tips (Digital Instruments; nominal spring constant 0.06 N m^{-1}). Two samples were analyzed. The raw images were subjected to first-order flattening, to correct for the nonlinear response of the piezo, and to fast Fourier transform filtering, to enhance surface regular structures. Flattening, filtering, and measurements of the rms roughness and the lattice parameters were performed with the accompanying Nanoscope IIIa software.

XRD. Three mica−titanium samples were analyzed with XRD. The mica was partially removed, leaving a few atomic layers on the titanium film, to reduce the strong signal from the mica and probe both the mica−titanium interface and the titanium film. One mica surface was also analyzed as a reference. A Bruker AXS D500 diffractometer with secondary monochromator was used to acquire the spectra presented here. The diffractometer was operated in the $\theta-2\theta$ arrangement, where θ is the angle between the incident X-rays and the sample surface and 2θ is the angle between incident and reflected X-rays. Large-angle-range survey spectra, with 2θ values ranging from 5° to 50°, were recorded with steps of 0.02° and a dwell time of 2.0 s/step. Unfiltered Cu Kα radiation was used, generated in a tube operating at 40 kV and 40 mA. The sample was rotated during analysis. Diffrac-AT software was used to process the results and subsequently compare them to the Joint Committee on Powder Diffraction Standards database.

SIMS. SIMS analyses of the Ti−mica interface were performed using a high mass resolution VG7035 magnetic sector SIMS instrument. Samples were placed in an ultrahigh-vacuum (10^{-7} Pa) chamber and biased at +4000 V relative to the mass spectrometer. A 25 keV field emission gallium liquid metal ion source (FEG UK) focused to a spot size of ~100 nm was used to raster scan the sample. For fast (300 s) and slow (2 h) etches, the primary ion source was operated at two currents, 2 and 5 nA over areas measuring 130 μm × 97 μm and 433 μm × 325 μm, respectively. Depth profiles (DP) were obtained for all ions of interest and background, using a noninteger mass, and were counted for 1 s each. The system requires 1 s to adjust between isotope counts; therefore, an analysis time of 6087 s (Figure 7) corresponds to 507 cycles of measurement. DP plots were acquired as a percentage of the full scale deflection (% FSD) of each element due to their different sensitivities (several orders of magnitude) in SIMS. FSD values could later be converted into counts per second (cps) using individual elemental factors provided by the system. These were then presented as semilogarithmic plots. Positive and negative secondary ions were detected in gating mode in order to eliminate crater edge effects. Specially written software operating under Microsoft Windows 95 was used to control the SIMS system and record spectra. Up to four rectangular areas per sample, spaced ~50 μm apart, were analyzed.

At each site, a broad surface scan (range 0−100 D) was acquired on a rectangular area of 1.4×10^{-3} cm^2 prior to depth profiling. The latter involved monitoring of a combination of ions, $^{48}Ti^{16}O^+$, $^{48}Ti^+$, $^{39}K^+$, $^{28}Si^+$, $^{27}Al^+$, and $^{16}O^+$. The first two ions were used to characterize the titanium oxide film, potassium, silicon, and aluminum ions acted as representatives of the mica phase, and $^{16}O^+$ was used to monitor the well-known oxygen enhancement effect which increases the secondary ion yields of electropositive elements. $^{60}TiC^+$ and $^{12}C^+$ were also included in some profiles because the former was detected in all wide scans and in the XPS investigations. During depth profiling for negative ions, $^{12}C^-$, $^{28}Si^-$, $^{16}O^-$, $^{27}AlO^-$, and $^{48}TiO^-$ were monitored.

XPS. Initially, two samples affixed to the glass supports were analyzed by XPS to study their surfaces. They were loaded into the spectrometer entry chamber immediately following mechanical removal of mica. After that, fresh samples of titanium on mica (no glass attached) were subjected to argon ion etching in order to depth profile through the titanium film from the as-deposited top surface and on into the mica beneath.

Analysis was conducted using an Escascope spectrometer (VG Scientific, East Grinstead, England). An unmonochromatized X-ray source equipped with a magnesium anode (Mg Kα = 1253.6 eV) operating at 300 W (15 kV and 20 mA) was used. The vacuum inside the spectrometer during analysis was ~10^{-7} Pa. The emitted photoelectrons were analyzed using a hemispherical energy analyzer, operating in the constant analyzer energy (fixed analyzer transmission) mode. Measurements were performed with an angle of 90° between the plane of the sample and the analyzer lens. The wide binding energy range survey spectra were obtained using an analyzer pass energy of 50 eV, while high-resolution spectra of selected energy intervals for the elemental chemical states of interest were taken at 30 eV pass energy. Argon ion etching for sample cleaning and depth profiling was performed using a VG Microtech EX05 ion gun fitted to the main analysis chamber of the spectrometer.

The XPS spectrum shows a laterally averaged composition of the analyzed area. For the surface spectra presented here, analysis areas of ~1.2 mm diameter were used. This was reduced to ~800 μm for the depth profiling experiments

(38) Hegner, M.; Wagner, P.; Semenza, G. *Surf. Sci.* **1993**, *291*, 39.

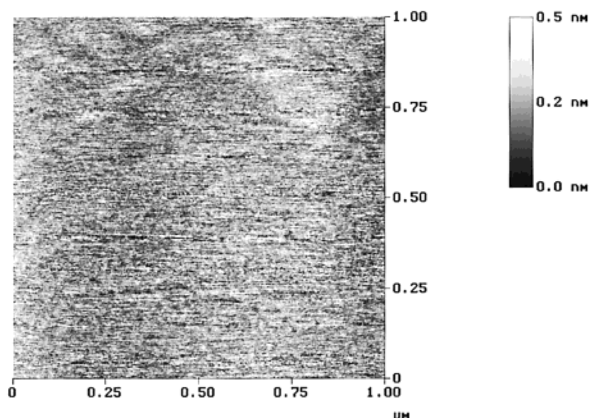

Figure 1. 1.00 μm × 1.00 μm AFM image of the exposed titanium surface showing the ultraflatness of the surface. rms = 0.29 ± 0.03 nm.

discussed below in order to fall within the etched area of the sample, minimizing so-called crater effects.

The atomic percentages of the elements and chemical states present on the analyzed surfaces and peak fits were calculated using the VGS5250 software and atomic sensitivity factors included with the instrument data system. Linear backgrounds were applied to the region spectra. The binding energies of the photoelectron peaks were referenced to the adventitious hydrocarbon peak C 1s at 284.8 eV. The error associated with XPS quantitative analysis may be taken to be ±10%.[39]

Results

AFM. Figures 1 and 2 present AFM images of the titanium surface after the removal of mica. Similar images were obtained on both of the investigated samples.

The 1.00 μm × 1.00 μm area presented in Figure 1 shows the flatness of the surface. The average rms roughness, calculated over five different 1.00 μm × 1.00 μm areas, was 0.29 nm ± 0.03 nm, similar to the rms of the flattest substrates normally used for AFM, such as mica and highly oriented pyrolytic graphite, which have a typical rms roughness of 0.1 nm.[40,41] At this scan size, no regular structures were observed. When the scanned area was reduced to 50.0 nm × 50.0 nm and below, some ordered structures were identified. These regular patterns were not stable under prolonged scanning. After the sample surface was scanned three to five times, the ordered surface appeared to be modified into a similar but distorted pattern, until eventually it disappeared. Upon enlarging the scan size centered on the same position, a hole was visualized in the central part of the image as a proof of the damage caused by the scanning tip (Figure 3). Surface ordered structures could be observed again by locating the AFM tip on a different surface area. However, the spacing and angles of the pattern changed in different areas. Furthermore, the occurrence, size, and spacing of ordered structures were not reproducible in different samples.

Undistorted and distorted square lattices as well as defects were observed in different areas and are shown in Figure 2a–c, respectively. The regular square lattice in Figure 2a has a spacing of a_0 = 0.49 nm and a 90° angle. Spacings of a_0 = 0.47 nm and b_0 = 0.35 nm with an angle of ~80° between a_0 and b_0 were observed in the lattice shown in Figure 2b. The ordered structure shown in Figure 2c exhibits some surface defects, denoting a lack of perfect cystallinity. The surface area occupied by different patterns varied. Some patterns extended over 50.0 nm × 50.0 nm areas, whereas others were observed only over 5.00 nm × 5.00 nm areas.

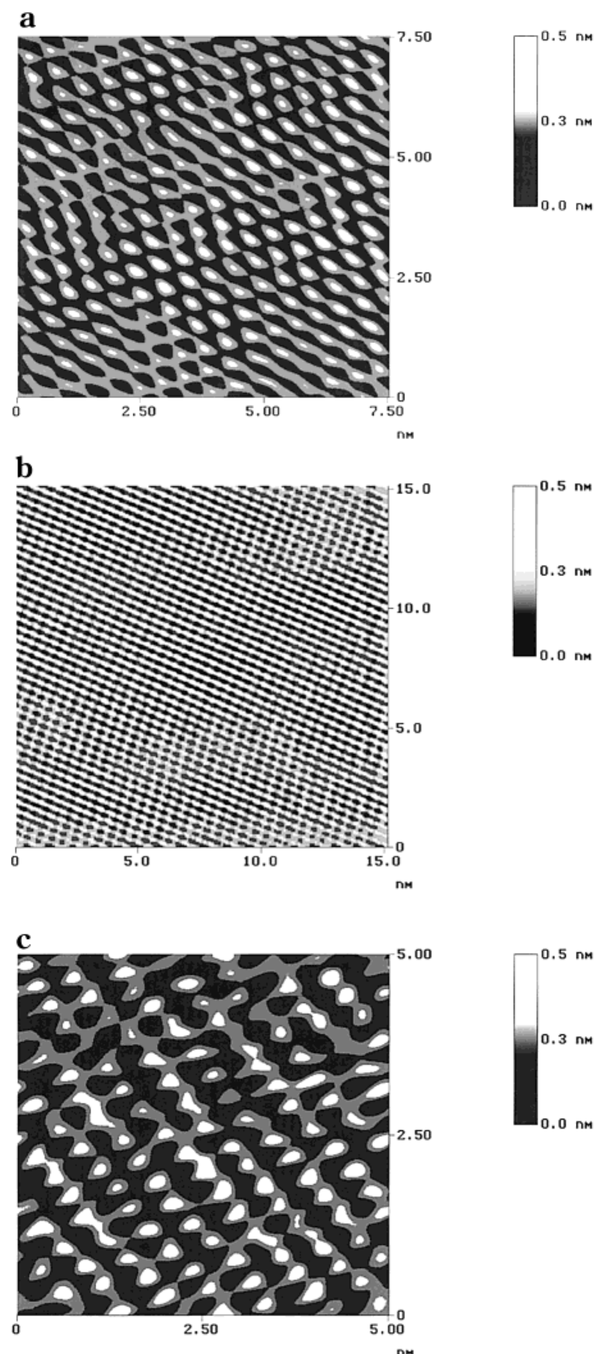

Figure 2. AFM images of the exposed titanium surface after removal of the mica: (a) surface region showing a regular square lattice; (b) surface region showing a distorted square lattice; (c) surface region showing defects within an ordered structure. The raw images, taken in contact mode in air, were filtered with inverse Fourier transform to enhance the ordered structure.

XRD. Figure 4 shows the $\theta-2\theta$ X-ray spectrum of mica. It shows the (003) reflection at the first and higher orders, as expected from the crystal structure of mica.

(39) Briggs, D. In *Handbook of X-ray and Ultraviolet Photoelectron Spectroscopy*; Heyden: London, U.K., 1977.
(40) Siedlecki, C. A.; Marchant, R. E. *Biomaterials* **1998**, *19*, 441.
(41) Siperko, L. M. *J. Vac. Sci. Technol. B* **1991**, *9*, 1061.

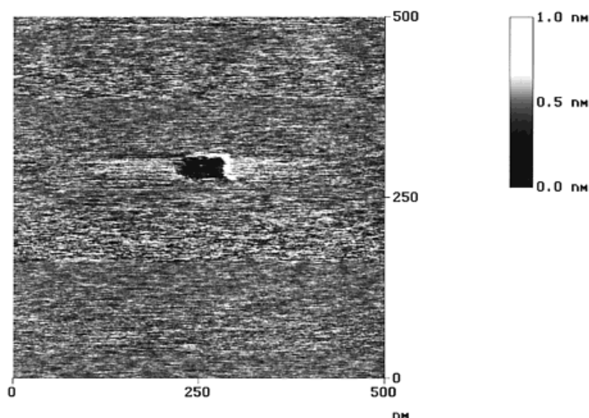

Figure 3. AFM image of the same sample shown in Figure 2 after a few scans. The hole in the central part of the image shows the damage caused by the tip to the sample surface.

Mica crystallizes with a sheet structure, with the sheets being held together by relatively weak bonds and resulting in a perfect basal cleavage of the mica. The unit cell is hexagonal with $a = 0.52$ nm and $c = 2.9988$ nm, and the cleavage plane is perpendicular to the c axis.[42]

Figure 5 shows the $\theta-2\theta$ X-ray spectrum of a mica–titanium sample, analyzed from the mica side. The mica substrate was partially removed before analysis. Only a thin layer of mica was left on the titanium film to reduce the background signal from the mica. Because of the smaller mica depth analyzed, compared to the spectrum presented in Figure 4, only the first three reflections from mica [(003), (006), and (009)] are clearly visible. These reflections gave a less intense signal compared to the mica peaks in Figure 4. In addition to the mica peaks, a peak at $2\theta = 38°$ is visible in Figure 5. This is attributed to the Ti(002) reflection from the titanium film. The crystal structure of titanium[3] is hexagonal with $a_0 = 0.295$ nm and $c_0 = 0.4686$ nm. Because the (001) reflection has a zero structure factor, the first observable reflection is (002).

SIMS. Parts a and b of Figure 6 show typical positive and negative spectra of the titanium surface on a semilogarithmic scale. The five naturally occurring isotopes of titanium dominated the positive ion spectra, where the central peak at mass 48 represents the most abundant titanium isotope. Molecular Ti derivatives included the oxide (TiO^+), dioxide (TiO_2^+), carbide (TiC^+), and diatomic (Ti_2^+) series, while only the hydride peak of $^{50}Ti^1H$ was visible, with the other lower mass hydrides being buried within the main Ti^+ cluster. Similarly, $^{48}Ti^{12}C^+$ (60 D) was another lone peak of the TiC series. Significant peaks common to all positive spectra were ^1H,^{23}Na,^{39}K, ^{40}Ca, and ^{41}K, as a result of environmental contamination, and, to a lesser extent, aliphatic hydrocarbons at $m/z = 13$, 15, 39, 41, 43, and 45. Also observed were peaks associated with impurities present in the deposited titanium wire, because SIMS is highly sensitive and capable of detecting trace elements at the parts-per-million to parts-per-billion (ppm–ppb) level. The main impurities (≥150 ppm) present in the titanium wire along with other contributing ions are listed in Table 2.

(42) Bailey, S. W. *Rev. Miner.* **1984**, *13*, 1.

Table 2. Main Impurities (≥150 ppm) Present in the Ti Wire with the Corresponding Concentrations Provided by the Supplier, the SIMS Peaks, and Other Species Contributing to the Same SIMS Peaks

element	concn in the titanium wire [ppm][a]	ions	m/z	other species with the same m/z
oxygen	2000	$^{16}O^+$	16	
		$^{18}O^+$	18	
		$^{32}O_2^+$	32	
iron	1500	$^{56}Fe^+$	56	$^{28}Si_2^+$
		$^{58}Fe^+$	58	$^{29}Si_2^+$
aluminum	300	$^{27}Al^+$	27	
carbon	300	$^{12}C^+$	12	
silicon	300	$^{28}Si^+$	28	$^{27}Al^1H^+$
		$^{29}Si^+$	29	
		$^{30}Si^+$	30	
nitrogen	150	$^{14}N^+$	14	CH_2^+

[a] Based on the supplier's typical estimation (Goodfellow Cambridge Ltd.).

It should be noted that Al^+ and Si^+ ions, chosen as representatives of mica in the DP, also exist as impurities. Aluminum has a variety of other fragments appearing at $m/z = 43$, 44, 59, 61, 70, and 86, corresponding to AlO^+, $AlOH^+$, AlO_2^+, $AlO_2H_2^+$, Al_2O^+, and $Al_2O_2^+$, respectively. A contribution to the peak at mass 61 was possible from $^{49}Ti^{12}C^+$. Si-derivative peaks occurred at $m/z = 45$, 56, and 58 because of $SiOH^+$, $^{28}Si_2^+$, and $^{29}Si_2^+$ respectively, although a minor contribution to the latter two peaks could have resulted from the iron impurity in the titanium film (Table 2). Finally, Ga^+ and GaO^+ at $m/z = 69$ and 85, respectively, are characteristic peaks arising from the implanted ions of the primary ion microprobe.

Negative spectra revealed relatively few peaks, with the predominant ones being H^-, C^-, O^-, and OH^-. Hydrocarbons, mainly in the form of CH^-, the environmental isotopes of Cl^-, and a low count of fluorine were the other peaks observed. F^- was not apparent in all surface spectra but, when present, did not exceed 30 cps, twice the background level.

Figure 7 shows a SIMS depth profile representative of the analyzed regions of the sample. The data for O^+, Al^+, Si^+, Ti^+, and TiO^+ were acquired over 507 cycles of measurement, equivalent to a time period of 6087 s. Not shown in the profile are background counts simultaneously acquired at a noninteger mass (7.6 D).

The well-known oxygen enhancement effect in SIMS is caused by the presence of the electronegative element oxygen, which acts as a yield-enhancing species for the electropositive elements that produce predominantly positive secondary ions, such as titanium.[43] The oxygen enhancement effect enabled the events of interest to be amplified in our samples (Figure 7). The initial decline of elements in the first 100 s is due to surface contamination followed by entry into the titanium film. At about 1700 s a steep rise in the Al^+ and Si^+ signal indicates encountering of a region rich in these ions. It is suggested here that this could be a diffusion zone where mica ions have interacted with the Ti film, probably during the thermal deposition process. The gradual rise in this diffusion zone culminates in a sudden drop in signal intensity, for all of the ions monitored, by several

(43) Storms, H. A.; Brown, K. F.; Stein, J. J. *Anal. Chem.* **1977**, *49*, 2023.

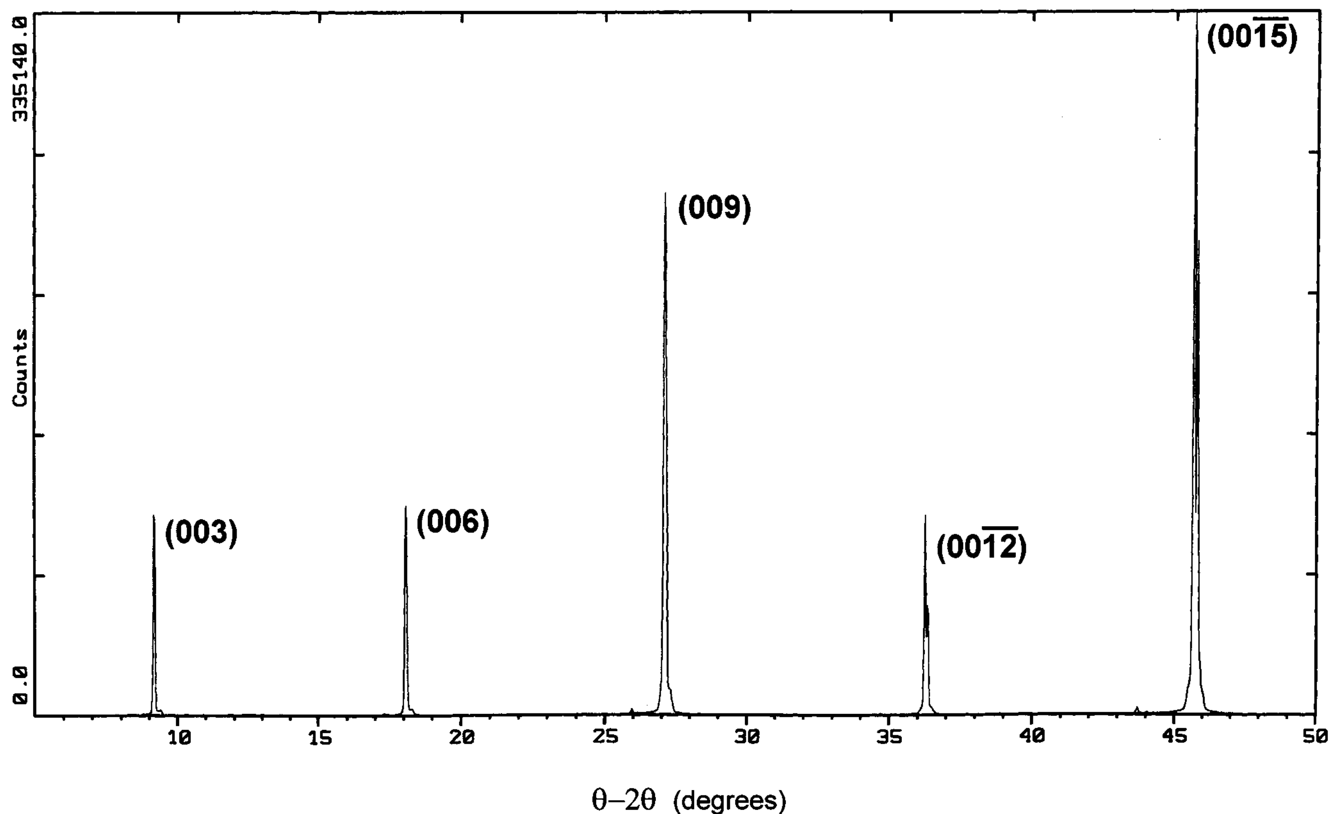

Figure 4. XRD spectrum of mica.

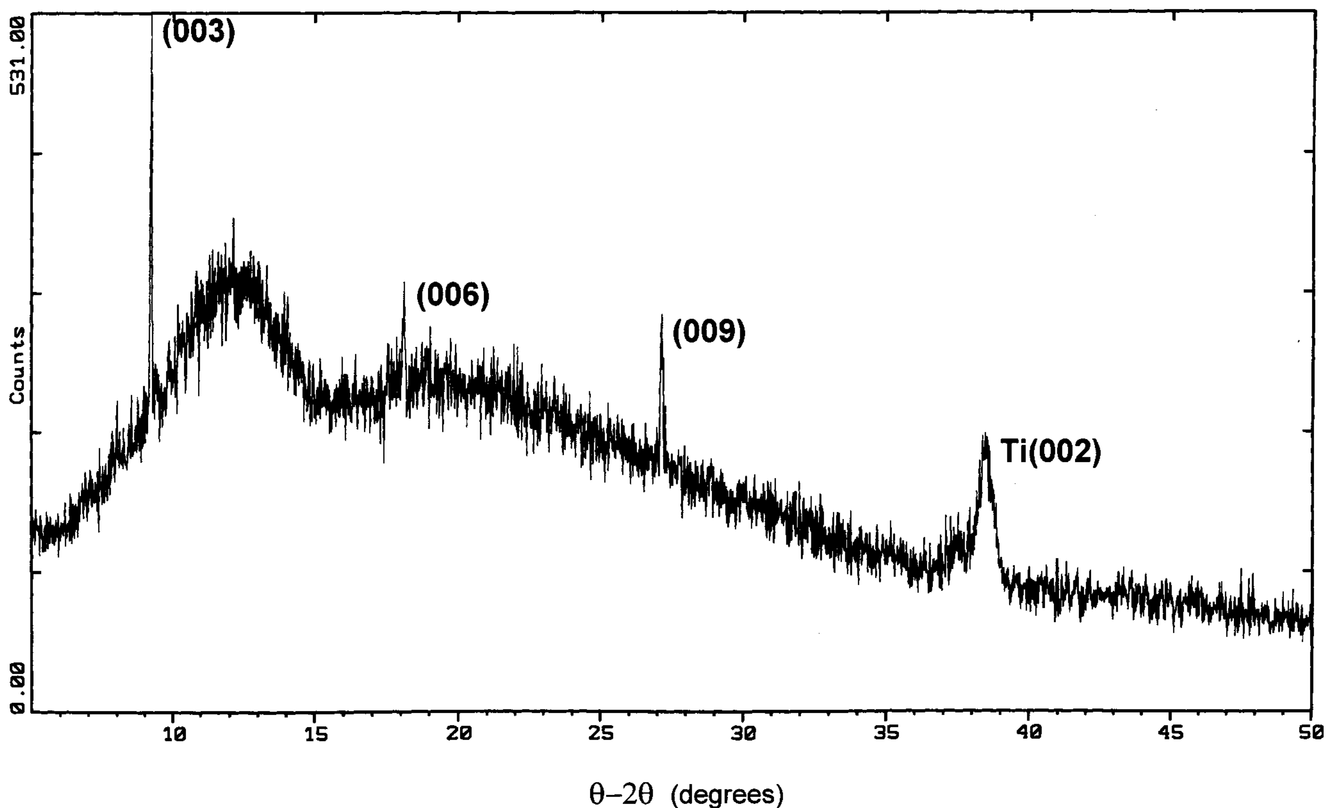

Figure 5. XRD spectrum of the mica–titanium sample. XRD investigation was conducted from the mica side.

orders of magnitude. The latter can be explained by the $^{69}Ga^{+}$ ion microprobe encountering the underlying mica surface, which, being an insulator, results in sample charging. Here, an excess of positive charges accumulates in the analysis region, repels the positive primary ion beam, and leads to a loss of counts. The attainment of the mica phase was observed after ~4200 s by the sudden increase in peak heights of $^{27}Al^{+}$ and $^{28}Si^{+}$ and the slight "hump" observed in the $^{16}O^{+}$ signal owing to mica being richer in oxygen than the Ti film.

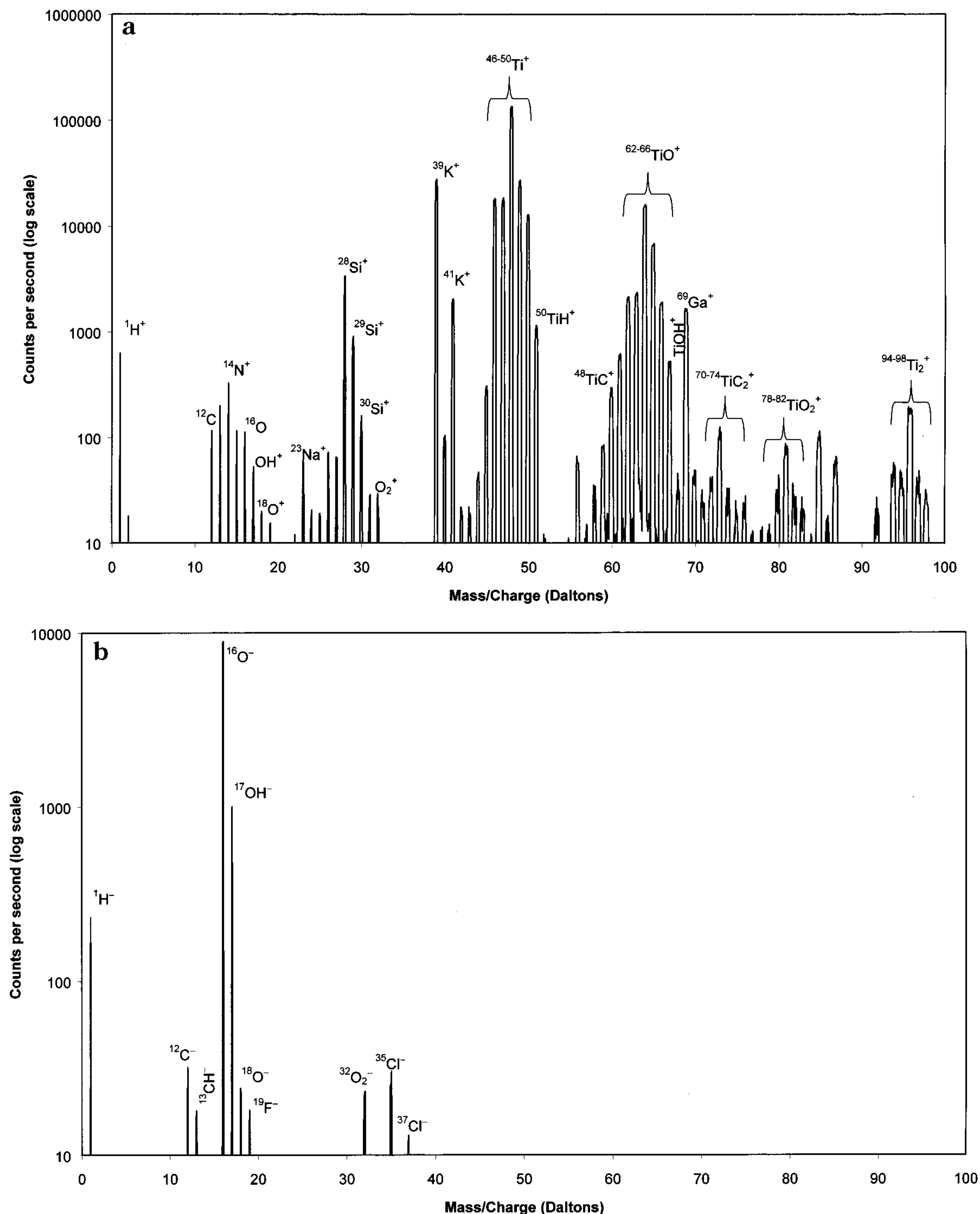

Figure 6. (a) Positive wide spectrum (0−100 Da) of a 1.4 × 10^{-3} cm^2 rectangular region of the sample surface prior to depth profiling of positive ions. (b) Negative wide spectrum (0−100 Da) of a different fresh 1.4 × 10^{-3} cm^2 rectangular surface region prior to depth profiling of negative ions.

In a different region on the same sample, $^{23}Na^+$ and $^{39}K^+$ signals were depth profiled for about 2 h and found to have a behavior similar to that of $^{27}Al^+$ and $^{28}Si^+$ (data not shown). Actual counts revealed Al^+ to be about 5 orders of magnitude higher than Si^+ for the data presented in Figure 7. However, taking into account their relative sensitivities in SIMS, where Si^+ is ~7 times less sensitive to detection, their counts amounted approximately to the same order of magnitude. The Ti^+ peak would have been expected to decrease upon reaching the interface. However, because of the diffusion and implantation of titanium ions into the substrate during ion bombardment and subsequent interaction with the highly reactive oxygen, Ti^+ remains constant, as verified by the complementary $^{48}Ti^{16}O^+$ peak monitored at $m/z = 64$.

At a different analysis site, TiC^+ and C^+ were monitored alongside Al^+, Ti^+, and their respective oxides (data not shown). The DP was acquired with the ion microprobe beam current set to 5 nA and scanned across a smaller analysis area, 130 μm × 97 μm. This led to a faster sample erosion rate and resulted in the events described above taking place over a much shorter time period, less than 300 s. The profiles of TiC^+ and C^+ were

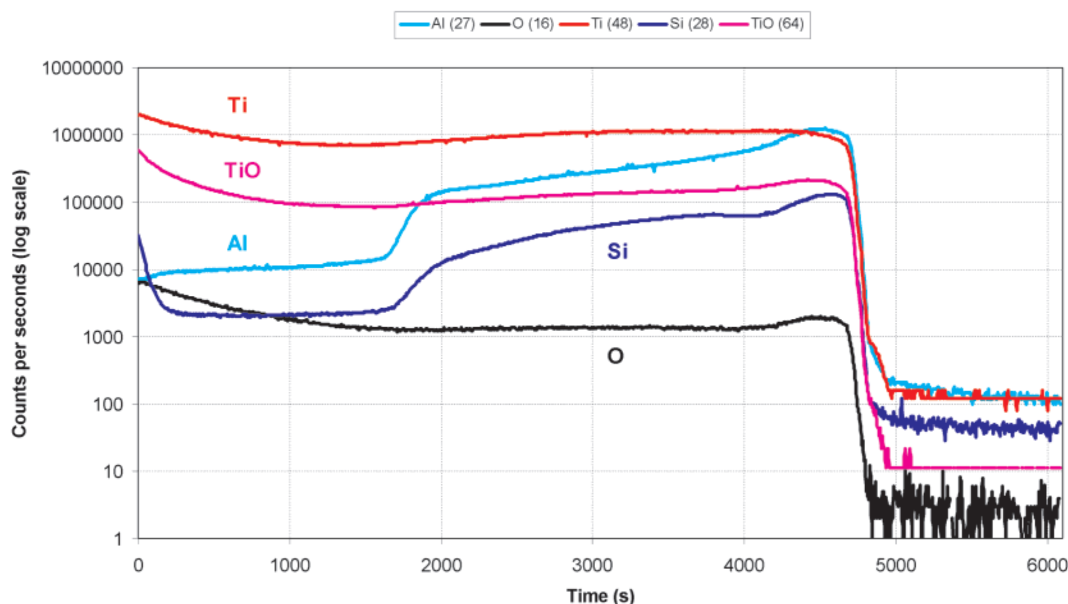

Figure 7. SIMS positive depth profile of a titanium–mica sample. The SIMS analysis started from the outer surface of the titanium side of the titanium–mica sample ($t = 0$ on the x axis).

of appearance similar to those of Ti^{+} and TiO^{+}. The system was then switched to negative secondary ion detection mode and C^{-}, Si^{-}, O^{-}, AlO^{-}, and TiO^{-} depth profiled at $m/z = 12$, 28, 16, 43, and 64 D under the same conditions on the same sample (data not shown). The ions were also profiled for ~2 h (6317 s) under the original conditions, i.e., beam current of 2 nA and analyzed area of 433 μm × 325 μm (data not shown). There was generally no change in the profiles of ions monitored in both positive and negative SIMS modes irrespective of the experimental conditions (current and analytical field of view) employed.

XPS. Figures 8 and 9 show the wide-scan XPS spectra of two samples before and after removal of the mica layer. Table 3 gives the corresponding chemical composition for each sample. Both samples exhibited similar results. Before the removal of mica, XPS detected carbon, oxygen, potassium, silicon, and aluminum, in similar atomic percentages in the two samples. Oxygen, potassium, silicon, and aluminum were detected because of the mica being present, with the binding energies of the peaks being as expected for the elements in this type of chemical environment.[44] The carbon was present as contamination, in both hydrocarbon and C–O species. A fluoride contamination of an unknown source was seen on the surface of one sample.

After removal of the mica (this was carried out outside the vacuum system, though the samples were reintroduced immediately after removal of the mica), only carbon, oxygen, and titanium were identified. Interestingly, the carbon concentrations were similar to those observed prior to removal. This could be due to the relatively poor vacuum present during the deposition process, allowing the entrapment of residual hydrocarbon species within the deposited titanium film. This is discussed in more detail below.

(44) Moulder, J. F.; Stickle, W. F.; Sobol, P. E.; Bomben, K. D. In *Handbook of X-ray Photoelectron Spectra—A Reference Book of Standard Spectra for Identification and Interpretation of XPS Data*; Chastain, J., Ed.; Perkin-Elmer Corp.: Eden Prairie, MN, 1992.

Table 3. XPS Chemical Analysis of Two Samples[a]

element	chemical states	atom %
	Sample 1	
	Before Mica Removal (Figure 8a)	
C	$-CH_2-$; $-CH_2-O-CH_2-$; >C=O	58.3
O	aluminosilicate (muscovite mica)	31.3
K	muscovite mica	2.0
Si	muscovite mica	3.7
Al	muscovite mica	3.9
F	fluoride	0.9
	After Mica Removal (Figure 8b)	
C	$-CH_2-$; $-CH_2-O-CH_2-$	59.0
O	hydroxide; TiO_2	28.6
Ti	TiO_2; Ti_2O_3	12.4
	Sample 2	
	Before Mica Removal (Figure 9a)	
C	$-CH_2-$; >C=O	62.9
O	aluminosilicate (muscovite mica)	28.3
K	muscovite mica	2.5
Si	muscovite mica	4.5
Al	muscovite mica	1.8
	After Mica Removal (Figure 9b)	
C	$-H_2-$; $-CH_2-O-CH_2-$; $-COOH$	55.1
O	hydroxide; TiO_2	33.0
Ti	TiO_2; Ti_2O_3	12.0

[a] For both samples the chemical compositions before and after mica removal and the measured atomic surface concentrations are given. The error associated with XPS quantification is ±10% of the measured value.[39]

The largest contribution to the titanium peak came from TiO_2. Ti_2O_3 was also detected on both samples,[34] in relatively small quantities. Figure 10 shows the fit obtained to the Ti 2p spectrum from one of the two samples, with contributions to the overall peak envelope from both TiO_2 (the major oxide present) and Ti_2O_3. A similar result was obtained for the other sample.

Argon ion etch depth profiling down through the titanium layer and on into the mica beneath showed a carbon and oxygen contamination overlayer on the surface, removed after the first three etch cycles (on the order of 30 nm; Figure 11). The carbon, oxygen, and titanium concentrations then remained constant until

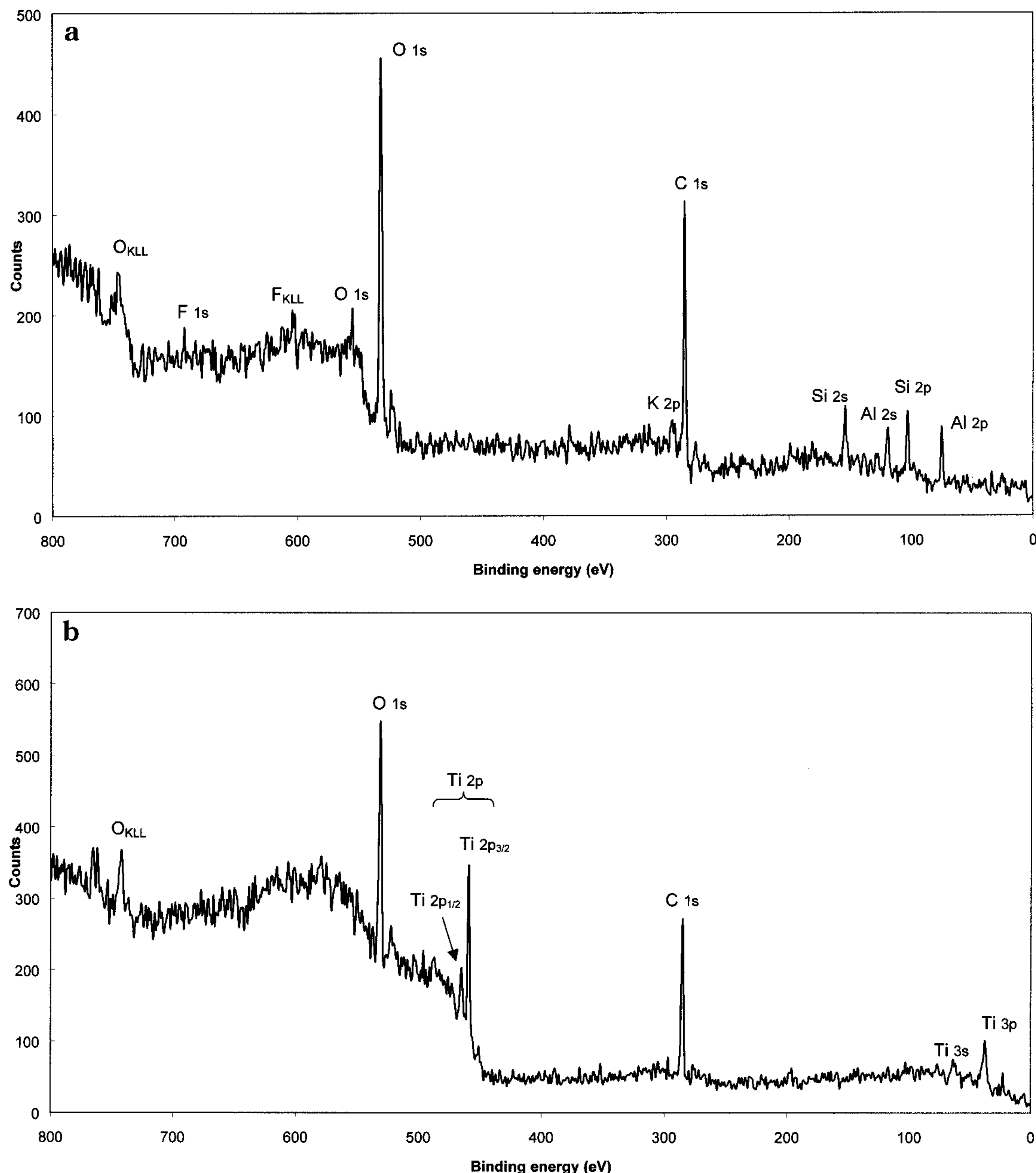

Figure 8. XPS spectra of the surface of sample 1: (a) before removal of mica; (b) after removal of mica.

the interface region above the mica was reached. Simultaneous to the reduction in titanium concentration, the oxygen level rose and silicon became apparent in the spectra. It is noteworthy that the carbon level dropped significantly from ~25−30 atom % down to zero. It is clear from this that any contribution to the carbon concentration in the earlier regions of the DP from residual hydrocarbons in the vacuum would have been minimal. Therefore, it would appear that the titanium was present, at least to some extent, as a carbide rather than the pure metal. The presence of the carbide is confirmed by a study of the C 1s region of the photoelectron spectra, where two peaks were seen, one due to adventitious hydrocarbon and the other, at a lower binding energy, attributed to titanium carbide (Figure 12).

For the depth profiled in this experiment, the titanium concentration never fell away to zero. This might be expected owing to the known knock-on effect of ion etching, pushing the surface titanium atoms deeper into the substrate mica than they would have been originally.

Discussion

The AFM investigation of the titanium surfaces obtained after removing mica from our samples revealed the presence of ordered structures, which could be readily damaged by the action of the AFM scanning tip. The coexistence of different crystalline forms of titanium oxide in the same sample was shown to be possible in a previous study where amorphous TiO_2 films were transformed into a mixture of TiO_2 anatase and rutile by laser annealing.[45] However, the different degrees of order observed in our AFM images could not always be assigned to well-defined crystalline lattices, nor were

(45) Hsu, L. S.; Solanki, R.; Collins G. J.; She, C. Y. *Appl. Phys. Lett.* **1984**, *45*, 1065.

Figure 9. XPS spectra of the surface of sample 2: (a) before removal of mica; (b) after removal of mica.

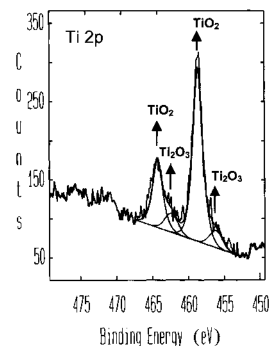

Figure 10. Fit to the Ti 2p region of the XPS spectrum of the surface of sample 1, showing contributions from both TiO_2 and Ti_2O_3.

they stable after a few scans. Therefore, they may be rather interpreted as different degrees of deformation of an original level of order. In our study, at least three different degrees of order were imaged. In addition to the regular square lattice with $a_0 = 0.49$ nm reported earlier[37] (Figure 2a), more detailed analysis showed the presence of a pattern with $a_0 = 0.47$ nm, $b_0 = 0.35$ nm, and an angle of $\sim80°$ (Figure 2b) and the presence of surface defects within a regular structure (Figure 2c). The square lattice in Figure 2a may correspond to the (001) plane of TiO_2 rutile (Table 1), whereas the patterns observed in Figure 2b and the presence of defects in Figure 2c may be interpreted as transition regions between different crystal structures or the result of disruption of the local order. High-resolution images similar to the one shown in Figure 2a were observed in different regions of the samples.

The following considerations allow us to rule out the possibility that the ordered structures observed in our AFM images corresponded to a residual mica layer covering the titanium film. It has been reported that the well-defined mica hexagonal lattice may not always appear at the surface imaged by AFM, because the

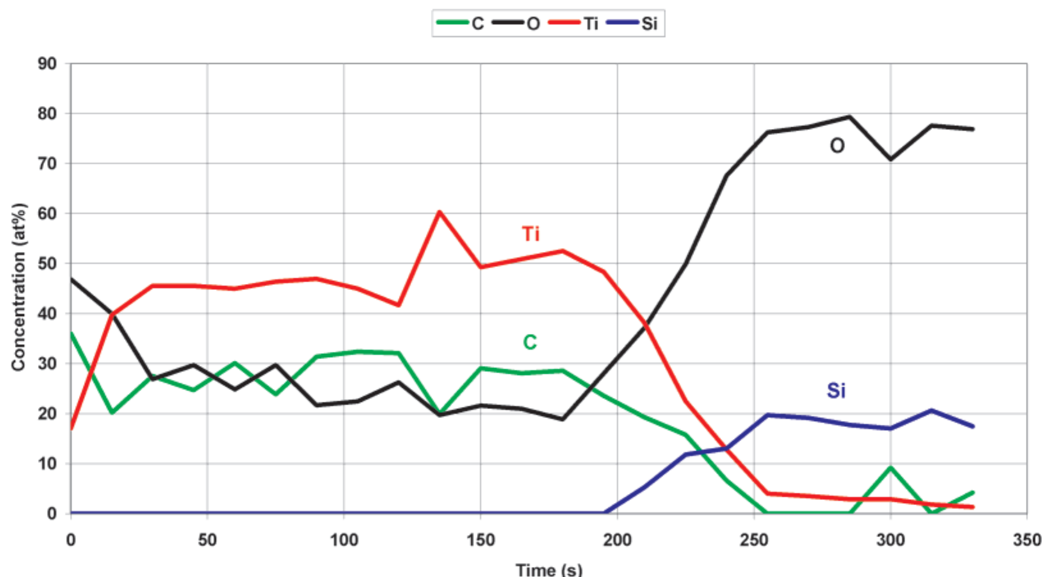

Figure 11. XPS depth profile of a titanium–mica sample. The XPS analysis started from the outer surface of the titanium side of the titanium–mica sample ($t = 0$ on the x axis).

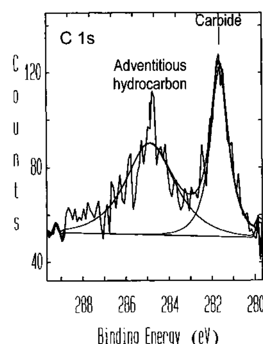

Figure 12. Fit to the C 1s region of the XPS spectrum acquired through the titanium film at $t = 105$ s during XPS depth profiling. The peak at higher binding energy results from the adventitious hydrocarbon, and the peak at lower binding energy is attributed to titanium carbide.

cleavage of mica may induce surface relaxation resulting from a rotation and/or tilting of the mica tetrahedral structure.[46,47] However, the removal of surface material observed after a few scans in our AFM images suggests that the imaged nonhexagonal structures may correspond to surface structures present at the interface between the mica and the titanium film rather than residual mica layers. It has indeed been shown that increasing scanning forces can induce surface relaxation[48] and removal of surface material from a mica surface.[49–51] However, the scanning forces needed to remove mica layers are in the order of a few hundred nano-Newtons,[49–51] which are larger than the forces normally involved in conventional AFM contact mode imaging with soft cantilevers such as those in our study, which are usually on the order of a few nano-Newtons.[52]

To complement the information provided by AFM imaging, the crystalline structure and the chemical composition of our samples were investigated with additional techniques. The ordered structures resolved by AFM were observed after the removal of mica, when the titanium film is exposed to ambient oxygen. However, under these conditions, a native, amorphous oxide layer should develop[1] and no crystalline structures would be expected on the surface. XRD analysis was conducted on titanium–mica samples to investigate the existence of crystalline structures in the bulk and to explore whether the crystalline structures at the interface between mica and titanium formed prior to mica removal or after exposure to ambient oxygen. The weak crystallization along the c axis of the bulk titanium films shown by XRD analysis of our samples was in agreement with the results of a previous study, which showed a weak crystallization along the c axis for titanium films prepared by thermal evaporation onto a mica substrate heated at 570 and 770 K.[34] Neither in that study nor in our samples were crystalline forms other than the bulk titanium and the mica substrate detected by XRD. In that study,[34] the interface between mica and titanium was not investigated. The ordered regions observed by AFM on the exposed titanium surface of our samples may have formed after the removal of mica and may have been induced by the ordered structures present in the titanium film. Because of the crystal order of the bulk titanium film, the first few layers of the native oxide forming after the removal of mica may arrange on the surface in a relatively ordered way to match the underlying ordered titanium film. The order of the growing oxide would then be progressively lost with the formation of following amorphous oxide layers. The different degrees of local order observed in our AFM images and the weakness of these regular structures may suggest the presence of very localized ordered titanium oxide(s) on the titanium film. This conclusion may also be supported by the results of the previously mentioned work,[34] which showed that highly oriented titanium oxides could be thermally grown only on underlying highly crystallized metallic titanium and

(46) Kuwahara, Y. *Phys. Chem. Miner.* **1999**, *26*, 198.
(47) Kuwahara, Y. *Phys. Chem. Miner.* **2001**, *28*, 1.
(48) Tang, H.; Joachim, C.; Devillers, J. *J. Vac. Sci. Technol. B* **1994**, *12*, 2179.
(49) Hu, J.; Xiao, X.-D.; Ogletree, D. F.; Salmeron, M. *Surf. Sci.* **1995**, *327*, 358.
(50) Popp, V.; Kladny, R.; Schimmel, T.; Kuppers, J. *Surf. Sci.* **1998**, *401*, 105.
(51) Miyake, S. *Appl. Phys. Lett.* **1995**, *67*, 2925.
(52) Shao, Z. F.; Mou, J.; Czajkowsky, D. M.; Yang, J.; Yuan, J.-Y. *Adv. Phys.* **1996**, *45*, 1.

that, even when the native titanium oxides were amorphous (i.e., grown on poorly crystallized titanium), the local octahedral environment of the oxygen atoms around the titanium atoms may have been preserved.

Even though XRD did not detect any crystalline form between the titanium film and the mica, a crystalline phase or a coexistence of different crystalline phases may have been present at the mica–titanium interface but may have been too thin to give a signal detectable by XRD, which is an averaging technique over several layers of material. These phases may have formed during the titanium deposition onto the mica surface in the vacuum chamber, and the first few depositing titanium layers may have been influenced by the underlying mica substrate and hence accommodated into ill-defined ordered structures onto the well-defined mica hexagonal structure, progressively adopting the hexagonal order of the bulk titanium film. These very local and thin ordered areas would then be exposed at the surface after the removal of mica and would be accessible to AFM imaging.

It is also possible that crystalline titanium oxides were present in films prior to mica removal. However, they may have been sparsely located or present in small amounts compared to the dominant crystalline pure titanium and, therefore, could not be detected by XRD. This is suggested by the additional information provided by the chemical investigation of the samples. Both SIMS and XPS depth profiling showed that the titanium films were not composed of pure titanium but contained a number of impurities, such as Si and Al, contained in the evaporating wire, and the environmental O and C present in the chamber probably as a result of the level of vacuum used for sample preparation. Titanium is highly reactive with oxygen and to a lesser extent with carbon.[1] Titanium atoms evaporating from the wire may have reacted with O and C atoms in the chamber and titanium–oxygen and titanium–carbon compounds may have deposited in the whole film, as suggested by the SIMS and XPS detections of titanium oxides and carbides throughout the films. The specific crystal or amorphous form assumed by titanium oxide is determined by the temperature at which titanium and oxygen react.[4] Because of the high temperatures present in the system during the sample preparation (such as 570 K on the mica surface and 2110 K in the melting titanium wire), titanium and oxygen may have formed crystalline rather than amorphous molecules when reacting in the chamber and depositing onto the mica surface. It cannot, therefore, be excluded that the ordered regions observed by AFM may be forms of crystalline titanium oxides.

Another interpretation for the ordered structures imaged at the titanium–mica interface can be suggested. At the beginning of the sample preparation, the mica surface is cleaved and placed in the vacuum chamber. A layer mainly composed of hydrocarbons forms on the freshly cleaved surface as a result of deposition of contaminants from the residual gases in the vacuum chamber. Hence, the titanium atoms may deposit on this hydrocarbon layer rather than on a "pure" mica surface. The AFM images may have visualized this labile contamination layer rather than the underlying titanium film.

Whatever the nature of the ordered structures observed by AFM, the main chemical composition of the titanium surfaces obtained after the removal of mica was titanium oxide, with TiO_2 the predominant form and Ti_2O_3 present in smaller amounts, as shown by XPS analysis. This fact and the flatness of these surfaces make these samples very useful for AFM investigation of biomolecules adsorption on a substrate that has chemical composition similar to the surfaces of currently used titanium implants, which are usually composed mainly of TiO_2 and other titanium oxides such as Ti_2O_3 as well as small percentages of contaminants such as C, Si, and Al, resulting from either the environment or the specific implant preparation process.[2,53] AFM investigations of biomolecules adsorbed on TiO_2 surfaces have been reported using titanium films evaporated onto a flat surface, such as mica or glass, and adsorbing the molecules on the titanium side of the film located at the opposite side of the substrate.[54] The advantages of the sample preparation method reported here are in the flatness of the titanium surfaces that are in contact with the mica and in the possibility of minimizing the surface contamination by exposing the titanium surface only when needed for investigation. The possibility that long storage times may result in a loss of flatness or in the contamination of the titanium–mica interface with elements diffusing from the mica or from the hypothesized carbon layer between the mica and the titanium film is currently under investigation in our laboratories.

Conclusions

Titanium oxide surfaces prepared by a novel method were shown to have a flat topography and a chemical composition similar to clinical implant surfaces. The first characteristic is required for high-resolution AFM imaging of adsorbed biomolecules, and the second is required to mimic the behavior of current biomaterial surfaces. Thus, the titanium oxide surfaces of this study were shown to be suitable substrates for the investigation of protein–biomaterial interactions at high resolution.

AFM imaging also revealed the presence of regions with different degrees of order on the surfaces. Complementary investigation of the sample bulks with XRD showed crystallized structures in the mica and titanium bulk film. On the basis of XRD results, the ordered regions observed by AFM at the mica–titanium interface were interpreted as locally crystallized forms of titanium oxides. Further evidence to this interpretation was given by the chemical analysis of the sample bulks. Both SIMS and XPS depth profiling detected O in the Ti film bulk regions as well as small amounts of contaminants, such as C, Si, and Al.

XPS analysis of the sample surfaces showed that the chemical composition was mainly TiO_2 with the presence of lesser percentages of Ti_2O_3 and small amounts of C, Si, and Al. This chemical composition is similar to the typical chemical composition of clinical titanium implant surfaces.[2,53]

(53) Cacciafesta, P.; Hallam, K. R.; Watkinson, A. C.; Allen, G. C.; Miles, M. J.; Jandt, K. D. *Surf. Sci.* **2001**, *491*, 405.
(54) Zenhausern, F.; Adrian, M.; Descouts, P. *J. Electron Microsc.* **1993**, *42*, 378.

The samples have the additional advantage of potential long-term storage with minimal risk of contamination or loss of flatness.

Acknowledgment. P.C. and K.D.J. gratefully acknowledge the partial support of the Non Medical Research Committee of the Special Trustees for the United Bristol Hospitals (Project 78); the Royal Society (Project 574006.G503/19680/JECL/SM); a University of Bristol Faculty of Medicine Research Scholarship; and Mike Weiss from Digital Instruments, Santa Barbara, CA. P.C. and K.D.J. also thank Dr. Peter Shellis (Department of Oral and Dental Science) for invaluable discussion and assistance and Drs. Marcus Textor and Ilya Reviakine (Laboratory for Surface Science and Technology, ETH Zürich, Zürich, Switzerland) for useful discussion. A.D.L.H. and M.J.M. gratefully acknowledge the support of EPSRC and IACR, Long Ashton. The authors gratefully acknowledge Dr. James S. Dalton, Dr. Charles M. Younes, and Mike Holt (Interface Analysis Centre) for useful discussions.

CM0112183